RSC Advances

PAPER

View Article Online
View Journal | View Issue

Cite this: *RSC Adv.*, 2018, **8**, 30040

Utilization of modified *Dioscorea opposita* Thunb. as a novel biosorbent for the adsorption of indigo carmine in aqueous solutions†

Yanzhuo Zhang, *[a] Jun Li,[b] Jing Zhao,[c] Yi-fei Zhang[a] and Jing Fan[a]

Received 14th June 2018
Accepted 30th July 2018

DOI: 10.1039/c8ra05106b

rsc.li/rsc-advances

It is important to identify efficient adsorbents for the removal of dyestuffs from aqueous solutions as this kind of pollution becomes more extensive. In this study, *Dioscorea opposita* Thunb. (DOT) was modified with polyethylene imine (DOT@PEI) as a novel biosorbent to remove the typical anionic dye indigo carmine (IC) from wastewater. The modified DOT@PEI biosorbent was characterized using BET (Brunauer–Emmett–Teller), SEM (scanning electron microscopy), EDS (energy dispersive spectroscopy), and FTIR (Fourier transform infrared spectroscopy) methods, and the results demonstrated that DOT@PEI is an excellent biosorbent. Batch adsorption studies showed that optimum adsorption parameters were pH 2.0, 1.0 g L^{-1} dosage, and temperature of 20 °C. The isothermal adsorption data showed good fitting to the Langmuir model, with a maximum adsorption capability of 344.83 mg g^{-1} for IC. Kinetic experiments showed that the experimental data fitted well to a pseudo-second-order kinetic model and the thermodynamic parameters indicated that adsorption is a spontaneous exothermic process. Adsorption–desorption experiments illustrated the good regeneration capability of DOT@PEI. These results demonstrate that DOT@PEI can be used as an effective biosorbent in water for the removal of anionic dyes such as required for environmental applications.

1 Introduction

Dyes are widely used in a variety of industries such as textiles, printing, food, paper, cosmetics, leather, and medicine. In China there is significant textile printing and dyeing, resulting in wastewater emissions of about (3–4) × 10^6 m^3 every day.[1] This kind of emission accounted for 35% of total industrial wastewaters and the rate of increase is more than 1%.[1] Complex organic compounds with aromatic rings and azo bonds are present in printing and dyeing wastewater.[2] Indigo carmine (IC) is an anionic dye that is widely used in food products, cosmetics, and drugs, and in many other industries.[3,4] IC may enter into the food chain and affect humans and animals by direct contact or inhalation.[5] Azo dyes and their decomposition products may introduce toxicity to aquatic environments, inducing cell mutations that can lead to cancer.[6] Therefore, the need to remove dyestuffs from industrial wastewater has become a significant issue. To address this, various physical and chemical methods like adsorption, photocatalytic processes, chemical coagulation, flocculation, precipitation, chemical oxidation, electrochemical oxidation, and biological processes have been described for the treatment of dyes.[7–9] Of these methods, chemical coagulation, electrochemical oxidation, and photocatalysis are not sufficiently effective for many dyes.[14–16] Adsorption is a common wastewater treatment technology, favored for its convenience and efficiency.[10–13]

Recently, the use of agricultural and forestry wastes as biosorbent materials for dye removal has attracted great attention due to the abundance, availability, and low cost of these materials. *Dioscorea opposita* Thunb. (DOT) tastes good, but the taste of the skin of DOT is unpleasant, so most people do not eat it.[17,18] Because DOT is a popular food, there is a large amount of the inedible DOT skin, making it a significant agricultural waste. If the DOT skin is discarded or burned, this may negatively impact the soil and atmospheric environment and is a waste of resources.[19] DOT has good specific surface area, and is abundant and inexpensive. One promising method to utilize this valuable bio-resource is to produce DOT-based biosorbents. A reasonable modification method can enhance the adsorption capacity of raw DOT to allow its use in anionic dye removal by binding, complexation, or electrostatic action.

Polyethylene imine (PEI) is a water-soluble polymer that can be used in water in its cationic form for the neutralization and adsorption of anionic material.[20] There is strong electrostatic interaction between PEI and particles that are negatively

[a]*School of Environment, Henan Normal University, Key Laboratory for Yellow River and Huai River Water Environmental and Pollution Control, Ministry of Education, Henan Key Laboratory for Environmental Pollution Control, Xinxiang, Henan 453007, P. R. China. E-mail: 83995983@qq.com*

[b]*The College of Architecture and Civil Engineering, The Key Laboratory of Beijing for Water Quality Science & Water Environment Recovery Engineering, Beijing University of Technology, Beijing 100124, China. E-mail: lijunbjut@163.com*

[c]*School of Chemistry and Chemical Engineering, Henan Normal University, Xinxiang, Henan 453007, P. R. China*

† Electronic supplementary information (ESI) available. See DOI: 10.1039/c8ra05106b

charged, so PEI molecules are attracted to a negatively charged surface. This allows PEI to be used in water treatment, in plating solutions, as a dispersing agent, and in other applications. In recent years, many studies have focused on the removal of heavy metal ions with the ability to chelate.[21–25] However, there has been little study of DOT modification with PEI for the removal of refractory organic pollutants, particularly the removal of anionic dyes. Here, we introduce a new biosorption material for use in dye removal.

DOT skin was modified with PEI (DOT@PEI) to make a potential biosorbent for the adsorption of IC in aqueous solution. The characteristics of the DOT@PEI material were measured using scanning electron microscopy (SEM), energy dispersive spectroscopy (EDS), Fourier transform infrared (FTIR) spectroscopy, and BET and zeta potential measurements. The adsorption process was optimized by varying the parameters of pH, dosage, and contact time. Analyses of isotherms, kinetics, and thermodynamics were used to describe the experimental data.

2 Materials and methods

2.1 Raw DOT and synthesis of modified DOT

The raw DOT was obtained from Jiaozuo, China. The sample (DOT skin) was washed several times with distilled water and ethanol to remove fly ash, dust, and other inorganic impurities. Next, the brown-colored DOT was dried in an oven at 60 °C for 48 h until reaching constant weight. Next, the DOT was crushed and screened to select powders of particle sizes of 0.2–0.5 mm. Finally, the obtained DOT was sealed and stored for further use or modification (Fig. 1a).

For the modification process, 10 mL of PEI (colloidal solution) was first added to a vessel with 1000 mL distilled water and stirred until the PEI solution was completely dissolved, producing a light-yellow viscous solution. Next, to this solution, 25 g DOT skin was added and mixed using a mechanical agitator at room temperature for 6 h. Finally, the modified DOT (DOT@PEI) was obtained by precipitation, suction filtration, and drying at 60 °C for 48 h. The color changed to deep brown after modification (Fig. 1b); after adsorption, the color changed from brown to red (Fig. 1c).

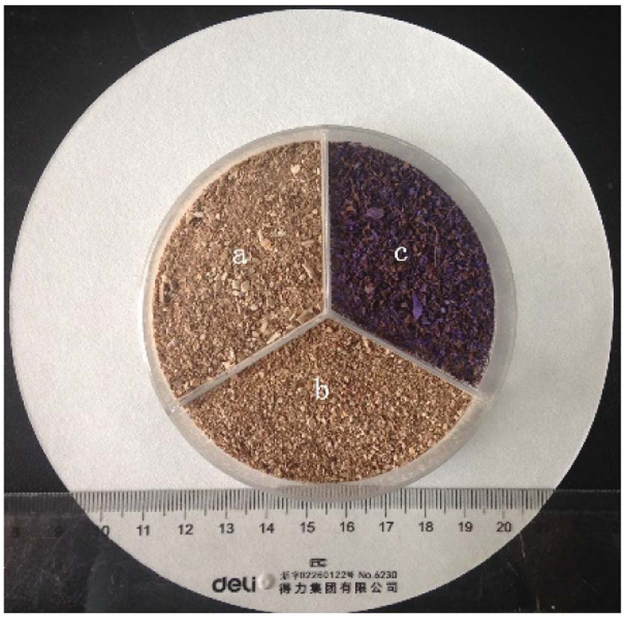

Fig. 1 (a) Image of raw DOT, (b) DOT@PEI and (c) DOT@PEI after adsorption.

2.2 Reagents and dyes

Anionic dye IC was obtained from Tianjin Fuchen Co. Ltd, China. The relevant parameters of IC are shown in Table 1. PEI (MW1800, 99% solution) was purchased from Shanghai Aladdin Co. Ltd, China. All the reagents used in the experiments were of analytic quality.

2.3 Instrumentation and analytical method

The residual concentration of IC was analyzed by measuring the absorbance values with an ultraviolet-visible spectrophotometer (UV-765, manufactured by Shanghai Precision and Scientific Instrument Co. Ltd) and the concentration of dye in solution was calculated according to the standard curve.

SEM and EDS were performed with a scanning electron microscope (Quanta 200, FEI, USA) operating at 30 kV.

The FTIR spectrometer, Alpha Infrared Spectrometer, was made by Bruker (Germany). Before and after the adsorption of dye to DOT@PEI, FTIR spectra were recorded at wavelengths ranging from 4000 to 500 cm^{-1}, with a resolution of 4 cm^{-1}.

Zeta potential was analyzed with a Zetasizer Nano2000 (Malvern Instruments, UK).

2.4 Batch adsorption tests

Dye adsorption tests were conducted in a conical flask containing 250 mL of dye solution, which was agitated in a water bath shaker with a shaking rate of 180 rpm at different temperatures until reaching equilibrium. Each experiment was maintained for 6 h. Samples were removed at certain time intervals, centrifuged at 3200 rpm for 2 min, and then analyzed by using a UV-765 spectrophotometer. During the static adsorption process, the pH of the solution was adjusted as necessary by addition of 1 M HCl or 1 M NaOH.

Table 1 The physical and chemical properties of indigo carmine

Name	Indigo carmine
Molecular formula	$C_{16}H_8N_2Na_2O_8S_2$
Number	466.37
Absorbance value	608
CAS number	860-22-0
Chemical structure	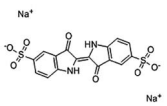

The effect of pH (2, 3, 4, 5, or 6) on dye removal was investigated by mixing 250 mL of dye solution at an initial dye concentration of 300 mg L^{-1} at 20 °C for 6 h. The effect of biosorbent dosage (1, 2, 3, 4, or 5 g L^{-1}) on dye removal was investigated by mixing 250 mL of dye solution at pH 2 with an initial dye concentration of 200 mg L^{-1} at 20 °C for 6 h. The change in dye concentration for all solution samples (100, 200, 300, 400, or 500 mg L^{-1}) was measured at certain time intervals (1, 3, 5, 10, 15, 20, 30, 50, 70, or 90 min) at pH 2 and 20 °C during adsorption.

After adsorption equilibrium was achieved, the adsorption capacity and removal rate (R) of the dye by DOT@PEI were computed as follows:

$$q_e = \frac{V(C_0 - C_e)}{M} \quad (1)$$

$$R = \frac{(C_0 - C_e)}{C_0} \times 100 \quad (2)$$

where q_e is the equilibrium adsorption capacity of the adsorbent, mg g^{-1}; C_0 is the initial concentration of the dye, mg L^{-1}; C_e is the liquid-phase dye concentration at equilibrium, mg L^{-1}; V is the volume of the solution, L; M is the dosage of the adsorbent, g.

2.5 Desorption and regeneration studies

To regenerate the used DOT@PEI biosorbent for further dye removal, regeneration tests were conducted with a batch method. First, exhausted DOT@PEI was obtained by immersing 1 g biosorbent into IC solution (200 mg g^{-1}). Subsequently, the exhausted DOT@PEI was added into sodium hydroxide solution to a concentration of 0.5 M, and then was shaken in a constant temperature water bath oscillator at room temperature for 2 h. The stripped DOT@PEI was neutralized with 1 M hydrochloric acid for another 2 h. Finally, the regeneration of exhausted DOT@PEI was evaluated by executing 5 successive regeneration cycles.

3 Results and discussion

3.1 Characteristics of the biosorbent

3.1.1 SEM analysis. The morphological structures of DOT and DOT@PEI were characterized by SEM as shown in Fig. S1.† Three samples were tested for each. The DOT was composed of cellulose and starch granules on its surface (Fig. S1a†). The raw DOT appears to have high porosity between the cellulose and starch granules. After being loaded with PEI, the surface of raw DOT was smoother because it became filled with PEI during the modification process, but its porous morphology remained (Fig. S1b†). The loaded PEI and numerous tiny pores facilitated dye collection and adsorption.

3.1.2 EDS analysis. The EDS spectrum of DOT is shown in Fig. S2(a)† and the elemental analysis results listed in Table S1† indicate that the raw DOT mainly consists of C and O, and trace amounts of Mg, Si, P, S, Cl, K, Ca, Fe, and Zn.[26] The large amount of C and O was attributed to the polysaccharides, starch, and crude fiber such as cellulose, hemicellulose, and lignin in DOT. After modification, the weight percentage of C was strongly increased. However, the peaks of O and other trace elements were slightly decreased, as shown in Fig. S2(b).† This phenomenon shows that DOT was modified successfully with PEI as a result of the introduction of amino groups.

3.1.3 FTIR analysis. DOT@PEI exhibited a significantly improved adsorption capacity relative to raw DOT. To further study the mechanism, we explored the surface functional groups of DOT@PEI and raw DOT by FTIR analysis in the range of 500–4000 cm^{-1}. Fig. S3(a)† shows the FTIR spectrum for the raw DOT. In Fig. S3(a),† the main spectral peaks of functional groups were found at 3358, 2928, 1733, 1646, 1383, 1158, 1243, 1048, 861, and 756 cm^{-1}. The distinct band at 3358 cm^{-1} may correspond to the O–H stretching vibration of cellulose and lignin.[27] The distinct band at 2928 cm^{-1} was attributed to the stretch vibration of C–H bond and the band at 1383 cm^{-1} was assigned to C–H bending vibrations in methyl and methylene groups. The peak at 1733 cm^{-1} was assigned to C=O stretching vibrations. The strong band at 1646 cm^{-1} can be ascribed to N–H bend vibrations. The peak at 1158 cm^{-1} was attributed to the C–O stretching vibration, indicating the presence of carboxyl groups on DOT. The peak at 1243 cm^{-1} and a weak band at around 1048 cm^{-1} may be due to C–O stretching vibrations in alcohol, phenol, or ether groups.[28]

Fig. S3b† shows the FTIR spectrum of the modified DOT@-PEI. There was no obvious change after modification except a slight change in the position of the main spectral peaks. The new band at 2359 cm^{-1} may correspond to the amino group ($-NH_2$), indicating that amino groups were successfully loaded on the surface of DOT@PEI. The peak at 1733 cm^{-1} disappeared after modification, possibly because the PEI occupied the active sites of the raw DOT. The new band at around 1457 cm^{-1} may be attributed to C–H bending vibrations in methyl and methylene groups. The 1418 cm^{-1} band may be due to C=C skeletal vibrations. Additionally, the strong peak of DOT@PEI at 1079 cm^{-1} and C–O–C band at around 1024 cm^{-1} confirmed the cellulose and lignin structures.

3.1.4 BET analysis. Fig. S4† shows the distribution of DOT@PEI pore size using the BJH model. Substitution of the measured values into the BET equation allowed the determination of a calculated surface area for DOT@PEI of 35.17 m^2 g^{-1}. The total pore volume and average pore diameter were 0.4518 cm^3 g^{-1} and 22.93 nm, respectively.

3.2 Factors affecting the adsorption of dye

3.2.1 Effect of pH value. The surface charge of DOT@PEI and the ionization degree of the dye are strongly affected by the solution pH.[29] Fig. 2 shows the relationship between q_e, removal rate and pH. The removal rate (R) and q_e of the anionic dye reached maximum values at pH 2. From pH 2 to 7, the adsorption capacities for the anionic dye significantly reduced. R was reduced from 91.08% to 49.49% and the value of q_e decreased from 182.17 to 83.18 mg L^{-1}. The value of q_e for DOT@PEI was almost 6.3 times higher than that for DOT. A pH of 2 was determined to be optimal, and this value was used for subsequent tests.

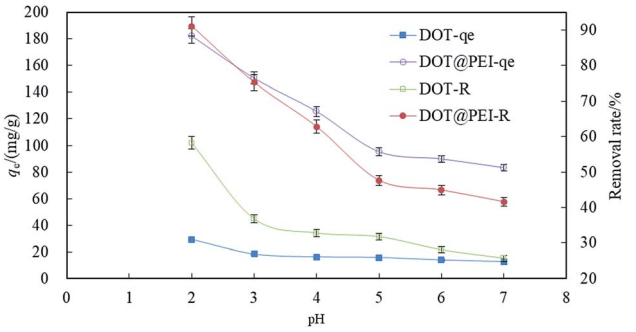

Fig. 2 The effects of pH on indigo carmine by DOT and DOT@PEI (T 20 °C, C_0 = 200 mg L^{-1}, dosage = 1 g L^{-1}, n = 5, error < ±3%).

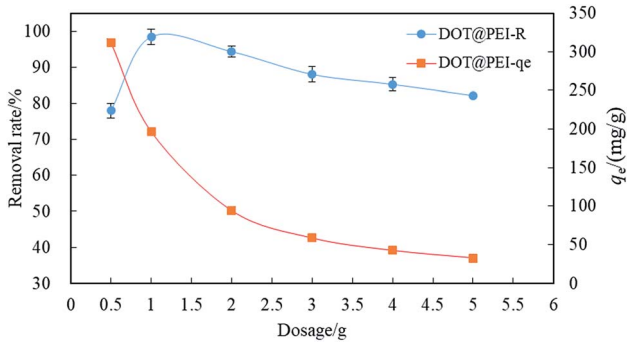

Fig. 3 The effect of biosorbent dosage on the removal efficiency of dye (pH = 2, T = 20 °C, C_0 = 200 mg L^{-1}, n = 5, error < ±3%).

The effect of the solution pH on dye uptake could be explained on the basis of zero charge point of DOT. The zeta potential of DOT and DOT@PEI were 2.2 and 7.1, respectively (Fig. S5†). During the removal of dyestuff *via* adsorption, pH can affect the solubility and coloring characteristics of the dyestuff in wastewater, the superficial electrification condition of the dye, and the de-coloration effect of DOT@PEI.

$$\text{Dye-SO}_3\text{Na} \xrightarrow{\text{H}_2\text{O}} \text{Dye-SO}_3^- + \text{Na}^+ \quad (3)$$

With the presence of H^+, the amino groups of modified DOT@PEI were protonated:

$$\text{DOT@PEI-NH}_2 + \text{H}^+ \rightleftharpoons \text{DOT@PEI-NH}_3^+ \quad (4)$$

The adsorption process then proceeded because of the electrostatic attraction between these two counter ions to a great extent:

$$\text{DOT@PEI-NH}_3^+ + \text{Dye-SO}_3^- \rightleftharpoons \text{DOT@PEI-NH}_3^+\text{O}_3\text{S-Dye} \quad (5)$$

According to eqn (3)–(5), when the dye is dissolved in an aqueous solution, the sulfonate (D-SO_3Na) separates and then transforms into anions. After acid treatment in the aqueous solution (pH 2), the positive ions of DOT@PEI are replaced by H^+; this process is called protonation of the adsorbent. Finally, the DOT@PEI-NH_3^+ with positive charge and the dye-SO_3^- with negative charge attract and bind each other resulting in the adsorption of anionic dye material by DOT@PEI. Similar conclusions were drawn in a study of adsorption of Acid Yellow 17 by aerobic granular sludge.[28] The experimental results indicated that adsorption was highest at pH 2.

3.2.2 Effect of biosorbent dosage and contact time. Fig. 3 shows the effect of biosorbent dosage on removal rate. The removal rate reached a maximum value at 1 g L^{-1} of DOT@PEI. The adsorption removal rate of IC increased sharply when the dosage of DOT@PEI increased from 0.5 to 1.0 g L^{-1}. When the dosage was increased from 1.0 to 5.0 g L^{-1}, R decreased slightly. However, q_e of biosorbent also decreased sharply from 312.06 mg g^{-1} to 32.89 mg g^{-1}. The increase of DOT@PEI amount provides more sites for the adsorption of the dyestuff and thus increases the removal rate. However, further increase in the biosorbent dosage leads to a reduction in the relative adsorption rate due to the agglomeration of biosorbent particles and an increase in diffusion path length.[30] At the same time, when the initial dye concentration is unchanged and removal rate improves, there are fewer dye molecules on the biosorbent. These results showed that the optimum DOT@PEI dosage was 1.0 g L^{-1}, which was used for the subsequent experiments.

Fig. 4 shows the relation between q_e and t for different initial concentrations of anionic dye. Most dye removal occurred before 30–50 min and adsorption equilibrium was reached at 90 min. During the first 30 min, the adsorbing rates of dye were highest and then the rate slowed down after 50 min. However, the maximum adsorption time and adsorption equilibrium time were not equivalent for different concentrations (100–500 mg g^{-1}). The maximum adsorption equilibrium times for low concentrations (100 and 200 mg g^{-1}) were 30 min and the maximum adsorption equilibrium times for the high concentrations (300, 400, and 500 mg g^{-1}) were 50 min.

The adsorption process reached equilibrium so quickly because adsorption mainly occurred on the surface of DOT@PEI. DOT@PEI has a very large superficial area and functional groups for the adsorption of dyes, facilitating the contact of dye molecules with the adsorption sites of the adsorbent. With time, the difference decreased gradually and the adsorption impetus was weakened, so the rate of adsorption was decreased and equilibrium was reached.

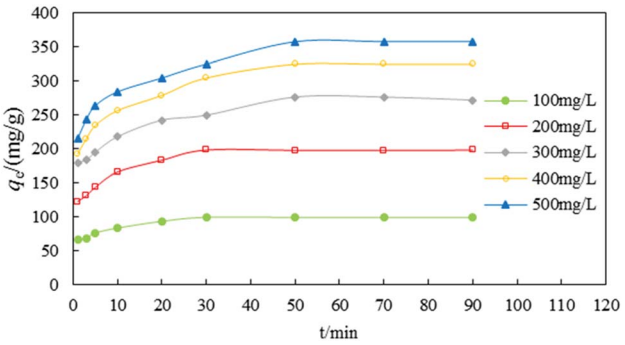

Fig. 4 The effect of contact time on the removal efficiency of dye (pH = 2, T = 20 °C, dosage = 1 g L^{-1}, n = 5, error < ±3%).

3.3 Adsorption isotherms

An adsorption isotherm represents how adsorption molecules reach the equilibrium state during the adsorption process for both liquid and solid phases. The time needed to reach the equilibrium state is called the adsorption equilibrium time. The balance between adsorption time and dye adsorption capacity reflects the saturated adsorption capacity of a biosorbent under the operating conditions. It is a very significant step to fit different isothermal adsorption models by data analysis, and finally to work out a best-fit model for the adsorption process.[19] Three adsorption isotherms, Langmuir model, Freundlich model and Temkin isotherm model, were used to fit the experiment data.

3.3.1 Langmuir adsorption isotherm. The assumed prerequisite of the Langmuir adsorption isotherm is that: the surfaces of the adsorbent are even and consist of a monomolecular layer; and no interaction force exists between the adsorbed molecules.[31]

$$\frac{1}{q_e} = \frac{1}{q_m} + \frac{1}{C_e \times b \times q_m} \quad (6)$$

In this case, C_e is the liquid-phase dye concentration at equilibrium, mg L^{-1}; q_e is the equilibrium adsorption capacity of the adsorbent, mg g^{-1}; q_m is the maximum adsorbing capacity, mg g^{-1}; b refers to the Langmuir constant, L mg^{-1}. Fig. S6† shows the equilibrium data in Langmuir isotherm expressions at 10, 20, 35 and 50 °C.

The experimental data are listed in Table 3 and describe the adsorption of the dye by DOT@PEI at 10, 20, 35 and 50 °C that were used to fit the Langmuir adsorption isotherm. The slope and intercept of a plot of $1/q_e$ *versus* $1/C_e$ allow determination of q_m and b. At concentrations of 100–500 mg L^{-1}, the experimental data fit the Langmuir adsorption isotherm during the adsorption process. From the data presented in Table 3, the q_m values of DOT@PEI for IC were 333.33, 344.83, 322.58, and 312.50 mg L^{-1} at 10, 20, 35, and 50 °C. This result indicates that the adsorption capacity was highest at 20 °C and the mean R^2 were 0.9950, 0.9937, 0.9990, and 0.9940 at 10, 20, 35, and 50 °C, respectively. The Langmuir adsorption isotherm was qualified to describe the experimental data.

The adsorption capacity of DOT@PEI was also compared with that of some other adsorbents. Table 2 presents the adsorption capacities of various kinds of adsorbents for IC. The adsorption capacities of DOT@PEI were much higher than those of the other adsorbents, including chitosan, modified starch, activated palm ash and so on.[32–36]

3.3.2 Freundlich adsorption isotherm. The Freundlich adsorption isotherm is an empirical equation to describe heterogeneous systems and adsorption capacity is based on the concentration of dyes at equilibrium. This isotherm is given by the following equation:

$$\ln q_e = \ln K_F + \frac{1}{n} \ln C_e \quad (7)$$

In this case, K_F is the Freundlich constant, (mg g^{-1}) (L $mg^{-1})^{1/n}$, which related to the adsorption capacity. If $0 < n^{-1} < 1$, the adsorption process is available and works well. Fig. S7† shows the equilibrium data for Freundlich isotherm expressions at 10, 20, 35 and 50 °C. The values of K_F and n are obtained from the intercept and the slope of a plot of ln q_e *versus* ln C_e.

The experimental data are listed in Table 3. Although $0 < n^{-1} < 1$ held over the whole temperature range for the dye, R^2 were in the range of 0.8460–0.9167. When n^{-1} ranges from 0 to 1, indicating uneven adsorption strength for the surface, surface adsorption can occur easily. The experimental data are within this concentration range, but the Freundlich adsorption isotherm deviated from the trend line. The experimental results showed that the Freundlich adsorption isotherm, used to describe a polymolecular layer, did not fit these data.

3.3.3 Temkin isotherm. The Temkin isotherm supposes that the adsorption heat decreases linearly rather than logarithmically, and concealed in the Freundlich equation. The Temkin isotherm is given the linear form:

$$q_e = B \ln A + B \ln C_e \quad (8)$$

where $B = RT/b$, T is the absolute temperature in K, R is the universal gas constant, 8.314 J (mol^{-1} K^{-1}), A is the equilibrium binding constant (L mg^{-1}) and B is related to the heat of adsorption.

The linear forms of Temkin isotherm plots are listed in Fig. S8.† The values of the Temkin parameters and R^2 were calculated from the intercept and the slope of a linear plot of q_e *versus* ln C_e. The Temkin constant B increased with increasing temperature up to 20 °C, then decreased, indicating exothermic adsorption.

Table 2 Adsorption capacities for indigo carmine of several adsorbents

Dye	Adsorbents	T/°C	q_m/(mg g^{-1})	Reference
Indigo carmine	Rice husk ash	30	29.3	32
	Zeolitic material	30	32.8	33
	Activated sewage sludge	25	60.0	34
	Pyrolysis of sewage sludge	30	92.8	32
	Nanocomposite hydrogels	30	370.4	35
	Magnetic NH_2-MIL-101(Al)	25	135.0	36
	DOT@PEI	20	344.83	This study

Table 3 Isotherm parameters for indigo carmine adsorption on DOT@PEI[a]

		Temperature/°C			
Dye	Parameters	10	20	35	50
Langmuir, the whole concentration range (100–500 mg L^{-1})					
Indigo carmine	q_m (mg g^{-1})	333.33	344.83	322.58	312.50
	b (L mg^{-1})	0.210	0.367	0.199	0.117
	R^2	0.9950	0.9937	0.9990	0.9940
Freundlich, the whole concentration range (100–500 mg L^{-1})					
Indigo carmine	K_F (mg g^{-1}) (L $mg^{-1})^{1/n}$	107.03	118.33	95.29	76.69
	n^{-1}	0.240	0.238	0.259	0.283
	R^2	0.8460	0.9016	0.8988	0.9167
Temkin, the whole concentration range (100–500 mg L^{-1})					
Indigo carmine	A (L mg^{-1})	1.575	2.298	1.490	0.721
	B	51.198	49.523	50.537	52.92
	R^2	0.9732	0.9742	0.9665	0.9724

[a] DOT@PEI dosage = 1.0 g L^{-1} and pH = 2.

As evident from Table 3, by comparison of R^2 values, we found that the values of R^2 for the Temkin isotherm (0.9732, 0.9742, 0.9665, and 0.9724 at 10, 20, 35 and 50 °C, respectively) were high, indicating that this model can be used to describe the adsorption process. However, compared with the Langmuir adsorption isotherm, the Temkin isotherm was not the best model in this experiment. The data calculated from the Temkin isotherm model show the heat of adsorption corresponding to physical adsorption.[37] However, by comparison of the correlation coefficients and other parameters, we found that the Langmuir isotherm was better qualified to describe the experimental data than the Freundlich and Temkin isotherms. These results are consistent with a model of anionic dye adsorption onto DOT@PEI *via* a monolayer adsorption process. In monolayer adsorption, BET plays a crucial part in adsorption, which explains the high adsorption capacity of DOT@PEI due to its large surface area and many functional groups.

3.4 Adsorption kinetics

In order to better describe the adsorption process, illustrate the adsorption process and explain the controlling principles from the perspective of kinetics, various kinetic models can be built. The chief models include pseudo-first-order kinetics, pseudo-second-order kinetics and intraparticle diffusion kinetics, and were used to study the reaction pathway and rate-controlling step during the adsorption of anionic dye by DOT@PEI.

3.4.1 Pseudo-first-order kinetic model. Pseudo-first-order kinetic model was presented by Lagergren[38] and expressed as follows:

$$\log(q_e - q_t) = \log q_e - \frac{k_1 t}{2.303} \quad (9)$$

where q_e is the experimental equilibrium adsorption capacity of the adsorbent, mg g^{-1}; q_t is the adsorption capacity during period t, mg g^{-1}; $q_{e.cal}$ is the theoretical equilibrium adsorption capacity, mg g^{-1}; k_1 is the pseudo-first-order kinetic model constant, 1/min.

Fig. S9† shows the relation between $\log(q_e-q_t)$ and t for different initial dyestuff concentrations. The constant was calculated from the isothermal linear slope and intercept and is shown in Table 4. We found that the $q_{e.cal}$ (5.17, 6.82, 7.41, 8.30 and 8.34 mg g^{-1}) values were lower than $q_{e.exp}$ (98.88, 196.76, 276.01, 324.69 and 354.66 mg g^{-1}), despite the high value of R^2 (0.9749–0.9950). This suggested that not all of the experimental data fitted the pseudo-first-order kinetic model. Therefore, this

Table 4 Kinetic model parameters for adsorption of indigo carmine by DOT@PEI at different initial concentrations[a]

		Pseudo-first-order kinetics			Pseudo-second-order kinetics				Intraparticle diffusion kinetics		
Dye	C_0	$q_{e.cal}$ (mg g^{-1})	k_1 (1/min)	R^2	$q_{e.cal}$ (mg g^{-1})	k_2 g (mg^{-1} min^{-1})	R^2	$q_{e.exp}$ (mg g^{-1})	k_3 ((mg g^{-1}) $min^{-1/2}$)	C	R^2
IC	100	5.17	0.118	0.9749	101.01	0.766	0.9997	98.88	4.1548	67.04	0.8156
	200	6.82	0.087	0.9950	200.00	0.338	0.9996	196.76	9.2452	126.27	0.8154
	300	7.41	0.047	0.9759	270.27	0.178	0.9958	276.01	10.6330	175.73	0.8845
	400	8.30	0.047	0.9718	333.33	0.136	0.9991	324.69	15.9740	196.00	0.9069
	500	8.34	0.060	0.9936	370.37	0.184	0.9987	354.66	16.8460	219.96	0.9219

[a] Temperature = 20 °C, DOT@PEI dosage = 1.0 g L^{-1} and pH = 2.

model cannot fully describe the whole adsorption process, but can describe the primary stage of adsorption.[39]

3.4.2 Pseudo-second-order kinetic model. Pseudo-second order kinetic model was proposed by Ho and Mckay, and can be used for in-depth analysis of kinetic data.[40] The model is expressed as:

$$\frac{t}{q_t} = \frac{1}{k_2 {q_{e2}}^2} + \frac{t}{q_e} \quad (10)$$

where k_2 is the pseudo-second-order kinetic model constant, g (mg^{-1} min^{-1}).

Fig. S10† shows the relation between t/q_e and t under different initial dyestuff concentrations. The constant k_2 can be calculated from the isothermal linear slope and intercept. As shown in Table 4, compared to the pseudo-first-order kinetic model, the calculated R^2 were closer to 1.000 for the pseudo-second-order kinetic model. Moreover, $q_{e.cal}$ showed good agreement with q_e, and the values were very similar; R^2 was between 0.9958 and 0.9997, indicating high correlation. The pseudo-second-order kinetic model better fitted the experimental data. The whole adsorption process was not fully described by the pseudo-first-order kinetic model, and this model is only able to describe the initial stage of the adsorption process. The pseudo-second-order kinetic model can describe well the whole adsorption process. Therefore, the pseudo-second-order kinetic model is suitable to describe the experimental data.

The comparison suggested that chemical adsorption was the rate-controlling step during the adsorption process of anionic dye by DOT@PEI. These conclusions indicated that chemical groups had a crucial effect between anionic dyestuff molecules and the surface of DOT@PEI, and that anionic dyestuff molecules were mainly adsorbed onto the surface of DOT@PEI.

3.4.3 Intraparticle diffusion model. The diffusion mechanism cannot be determined by pseudo-first-order or pseudo-second-order kinetic models, but was further analyzed to calculate the rate parameters of intraparticle diffusion. The equation is given by:

$$q_t = k_3 t^{1/2} + C \quad (11)$$

where k_3 ((mg g^{-1}) $min^{-1/2}$) is the internal granule diffusion speed constant; C is the intercept; the values of q_t and $t^{1/2}$ can be calculated from k_3, C and R^2. Details are shown in Fig. S11.†

Table 4 shows that k_3 and C both increased as the initial concentration was increased, which indicated that the internal diffusion rate increased with increased initial concentration for anionic dyes. The increase of initial concentration will lead to a higher concentration gradient, and eventually to faster diffusion and quicker adsorption. The curve can be divided into two parts: a nearly vertical part (membrane diffusion) and a slowly rising and equilibrium part (in-granule diffusion and adsorption equilibrium). The calculated data show that intraparticle diffusion is not the only component of the rate-controlling step. The initial step section ($t^{1/2}$ = 0–1 $min^{1/2}$) was very quick because the dye molecules transferred from the liquid phase to the adsorbent *via* membrane diffusion. The second section was from 1 ($t^{1/2} = 1$ $min^{1/2}$) to 90 min ($t^{1/2} = 9.4868$ $min^{1/2}$), and the dye molecules diffused from the aqueous solution into the mesopores of DOT@PEI by intraparticle diffusion. Therefore, the overall adsorption process can be considered as a combination of internal diffusion and membrane diffusion. On comparison of R^2 and other parameters (0.8154–0.9219) for the pseudo-first-order and pseudo-second-order kinetic model, the experimental data can be well described by the pseudo-first-order kinetic model.

3.5 Adsorption thermodynamics

Thermodynamic parameters are important indicators for the application of the adsorption process, including Gibbs free energy (ΔG^0), enthalpy change (ΔH^0) and entropy change (ΔS^0):

$$\Delta G^0 = -RTK_d \quad (12)$$

$$\ln K_d = \frac{\Delta S^0}{R} - \frac{\Delta H^0}{RT} \quad (13)$$

$$K_d = \frac{q_e}{C_e} \quad (14)$$

$$\Delta G^0 = \Delta H^0 - T\Delta S^0 \quad (15)$$

where R is the universal gas constant (8.314 J (mol^{-1} K^{-1})), T is the temperature (K) and K_d is the distribution coefficient. K_d was calculated according to eqn (14), ΔH^0 and ΔS^0 were calculated using eqn (13) from the slope and intercept of a plot of ln K_d *versus* $1/T$, respectively.

According to eqn (12)–(15) and Table 5, for all cases, the values of ΔG^0 and ΔH^0 were negative, which indicated that the adsorption may be a spontaneous exothermic process. If ΔS^0 were to be positive during the adsorption process, the degree of disorder increased at the interface between solid and liquid phases. In contrast, negative values of ΔS^0 illustrated that the change in ΔH^0 played a dominant role in contributing to the negative values of ΔG^0. In conclusion, the adsorption of anionic dye by DOT@PEI is a spontaneous exothermic process.

3.6 Regeneration of exhausted DOT@PEI

Excellent regeneration capability is crucial for an adsorbent after adsorption of dyes, promoting the reuse of the adsorbent for dye removal. For the IC used in this work, batch

Table 5 Thermodynamic parameters of anionic adsorption by DOT@PEI

	C_0	ΔG^0 (kJ mol^{-1})			ΔH^0	ΔS^0
Name	(mg L^{-1})	20 °C	35 °C	50 °C	(kJ mol^{-1})	(J (mol K)$^{-1}$)
IC	100	−10.91	−9.72	−8.65	−32.99	−75.42
	200	−10.00	−8.29	−7.42	−35.38	−87.04
	300	−5.95	−5.33	−3.96	−25.23	−65.43
	400	−3.56	−3.17	−2.80	−11.01	−25.44
	500	−2.17	−1.45	−1.23	−11.47	−31.98

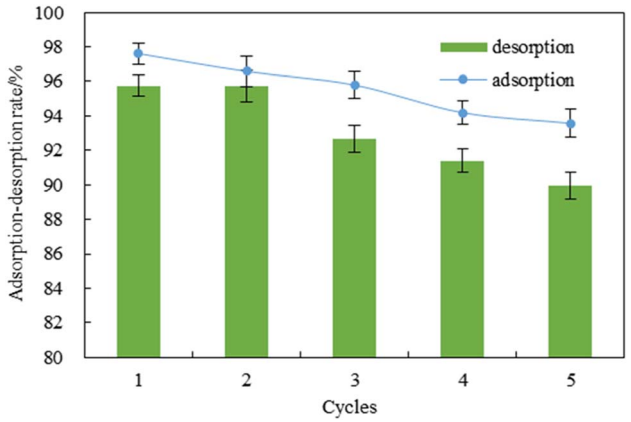

Fig. 5 Regeneration of indigo carmine from DOT@PEI for five adsorption–desorption cycles (pH = 2, T = 20 °C, dosage = 1 g L^{-1}, C_0 = 200 mg L^{-1}, n = 5, error < ±3%).

regeneration was carried out with sodium hydroxide solution (0.5 M). The results showed that IC was removed from the biosorbent after 2 h. The mean values of adsorption efficiency (R) were 95.55% for five adsorption–desorption cycles (Fig. 5). After that, the desorption rate was 93.10%. This demonstrated that the adsorption efficiency (mean value > 95%) and regeneration capability (mean value > 93%) were decreased slightly after five successive regeneration cycles.

4 Conclusion

DOT was successfully modified with PEI for use as a novel biosorbent to remove IC in aqueous solution. The maximum adsorption capacity was 344.83 mg g^{-1} for IC, mainly due to the porous structure of DOT@PEI and its abundance of functional groups. The equilibrium data fitted very well to the Langmuir model and the pseudo-second-order kinetic model. The thermodynamic parameters indicated that the adsorption was a spontaneous and exothermic process. Overall, the results indicated good adsorption capability of DOT@PEI, demonstrating that this material is an inexpensive and effective biosorbent for anionic dye removal in wastewater treatment.

Conflicts of interest

There are no conflicts to declare.

Acknowledgements

The work was supported by the Youth Science Foundation of Henan Normal University (2017QK22); the PhD established project of Henan Normal University (5101219170125); Key Scientific Project of University in Henan Province (19A610005).

References

1 R. C. Dai, T. Zhang, Q. Guo, J. W. Cao and Y. Jiang, Summary of printing-dyeing wastewater treatment technology, *Water and Wastewater Engineering*, 2000, **26**, 33–37.
2 Y. Li, H. Y. Yang, J. Y. Shen, Y. Mu and H. Q. Yu, Enhancement of azo dye decolourization in a MFC–MEC coupled system, *Bioresour. Technol.*, 2016, **202**, 93–100.
3 T. A. Saleh, *Nanomaterial and polymer membranes*, Elsevier, 2016, ISBN-13: 978-0128047033.
4 T. A. Saleh, *Advanced nanomaterials for water engineering, treatment, and hydraulics (advances in environmental engineering and green technologies)*, IGI Glob., 2017, ISBN-13: 978-1522521365.
5 G. Skouteris, D. Saroj, P. Melidis, F. I. Hai and S. Ouki, The effect of activated carbon addition on membrane bioreactor processes for wastewater treatment and reclamation – a critical review, *Bioresour. Technol.*, 2015, **185**, 399–410.
6 T. Maneerung, J. Liew, Y. Dai, S. Kawi, C. Chong and C. H. Wang, Activated carbon derived from carbon residue fro biomass gasification and its application for dye adsorption: kinetics, isotherms and thermodynamic studies, *Bioresour. Technol.*, 2016, **200**, 350–359.
7 H. C. Tao, H. R. Zhang, J. B. Li and W. Y. Ding, Biomass based activated carbon obtained from sludge and sugarcane bagasse for removing lead ion from wastewater, *Bioresour. Technol.*, 2015, **192**, 611–617.
8 T. A. Saleh, Nanocomposite of carbon nanotubes/silica nanoparticles and their use for adsorption of pb(II): from surface properties to sorption mechanism, *Desalin. Water Treat.*, 2015, **57**, 1–15.
9 H. A. Sani, M. B. Ahmad and T. A. Saleh, Synthesis of zinc oxide/talc nanocomposite for enhanced lead adsorption from aqueous solutions, *RSC Adv.*, 2016, **6**, 108819–108827.
10 V. K. Gupta, I. Ali, T. A. Saleh, A. Nayak and S. Agarwal, Chemical treatment technologies for waste-water recycling—an overview, *RSC Adv.*, 2012, **2**, 6380–6388.
11 H. A. Sani, M. B. Ahmad, M. Z. Hussein, N. A. Ibrahim, A. Musa and T. A. Saleh, Nanocomposite of ZnO with montmorillonite for removal of lead and copper ions from aqueous solutions, *Process Saf. Environ. Prot.*, 2017, **109**, 97–105.
12 A. M. Alansi, W. Z. Alkayali, M. H. Al-Qunaibit, T. F. Qahtan and T. A. Saleh, Synthesis of exfoliated polystyrene/anionic clay mgal-layered double hydroxide: structural and thermal properties, *RSC Adv.*, 2015, **5**, 71441–71448.
13 R. Soury, M. Jabli, T. A. Saleh, W. S. Abdul-Hassan, E. Saint-Aman, F. Loiseau, C. Philouze and H. Nasri, Tetrakis(ethyl-4(4-butyryl)oxyphenyl)porphyrinato zinc complexes with 4,4′-bpyridin: synthesis, characterization, and its catalytic degradation of calmagite, *RSC Adv.*, 2018, **8**, 28143–29156.
14 D. Morshedi, Z. Mohammadi, M. M. A. Boojar and F. Aliakbari, Using protein nanofibrils to remove azo dyes from aqueous solution by the coagulation process, *Colloids Surf., B*, 2013, **112**, 245–254.
15 G. Ramírez, F. J. Recio, P. Herrasti, C. Ponce-de-León and I. Sirés, Effect of RVC porosity on the performance of PbO_2 composite coatings with titanate nanotubes for the electrochemical oxidation of azo dyes, *Electrochim. Acta*, 2016, **204**, 9–17.

16 Q. Chen and Q. Wu, Preparation of carbon microspheres decorated with silver nanoparticles and their ability to remove dyes from aqueous solution, *J. Hazard. Mater.*, 2015, **283**, 193–201.
17 X. F. Feng, L. Q. Huang, X. G. Ge, L. J. Yang and J. Y. Yang, Textual research on origin and development of genuine medicinal herbs of Shanyao, *China J. Chin. Mater. Med.*, 2008, **33**, 859–862.
18 B. Gao, Y. Li and Z. Chen, Adsorption behaviour of functional grafting particles based on polyethyleneimine for chromate anions, *Chem. Eng. J.*, 2009, **150**, 337–343.
19 M. Ahmad, S. Ahmed, B. L. Swami and S. Ikram, Adsorption of heavy metal ions: role of chitosan and cellulose for water treatment, *Langmuir*, 2015, **2**, 280–289.
20 M. Owlad, M. K. Aroua and W. M. A. W. Daud, Hexavalent chromium adsorption on impregnated palm shell activated carbon with polyethyleneimine, *Bioresour. Technol.*, 2010, **101**, 5098–5103.
21 C. Y. Yin, M. K. Aroua and W. M. A. W. Daud, Impregnation of palm shell activated carbon with polyethyleneimine and its effects on Cd^{2+} adsorption, *Colloids Surf., A*, 2007, **307**, 128–136.
22 Y. Zhou, H. Guo and J. Zhou, Study on Main Nutrients in Iron *Dioscorea opposita* Thunb, *Food and Nutrition in China*, 2011, **17**, 69–71.
23 E. Garnier, P. Gravereau and A. Hardy, Zeolitic iron cyanides: the structure of $Na_2Zn_3[Fe(CN)_6]_2 \times H_2O$, *Acta Crystallogr., Sect. B: Struct. Sci.*, 1982, **38**, 1401–1405.
24 P. Wang, L. Tang, X. Wei, G. Zeng, Y. Zhou, Y. Deng, J. Wang, Z. Xie and W. Fang, Synthesis and application of iron and zinc doped biochar for removal of p-nitrophenol in wastewater and assessment of the influence of co-existed Pb(II), *Appl. Surf. Sci.*, 2016, **392**, 391–401.
25 L. Tang, J. Yu, Y. Pang, G. Zeng, J. Wang, X. Ren, S. Ye, B. Peng and H. Feng, Sustainable efficient adsorbent: alkali-acid modified magnetic biochar derived from sewage sludge for aqueous organic contaminant removal, *Chem. Eng. J.*, 2018, **336**, 160–169.
26 C. H. Tsai, W. C. Chang, D. Saikia, C. E. Wu and H. M. Kao, Functionalization of cubic mesoporous silica SBA-16 with carboxylic acid *via* one-pot synthesis route for effective removal of cationic dyes, *J. Hazard. Mater.*, 2015, **309**, 236–248.
27 M. M. Alshalalfeh, T. A. Saleh and A. A. Alsaadi, Silver colloid and film substrates in surface-enhanced raman scattering for 2-thiouracil detection, *RSC Adv.*, 2016, **6**, 75282–75292.
28 J. F. Gao, Q. Zhang, K. Su, R. Chen and Y. Z. Peng, Biosorption of Acid Yellow 17 from aqueous solution by non-living aerobic granular sludge, *J. Hazard. Mater.*, 2010, **174**, 215–225.
29 S. H. Chen, Q. Y. Yue, B. Y. Gao and X. Xu, Equilibrium and kinetic adsorption study of the adsorptive removal of Cr(VI) using modified wheat residue, *J. Colloid Interface Sci.*, 2010, **349**, 256–264.
30 V. Nair and R. Vinu, Peroxide-assisted microwave activation of pyrolysis char for adsorption of dyes from wastewater, *Bioresour. Technol.*, 2016, **216**, 511–519.
31 W. Song, B. Gao, X. Xu, L. Xing, S. Han, P. Duan and R. Jia, Adsorption–desorption behavior of magnetic amine/Fe_3O_4 functionalized biopolymer resin towards anionic dyes from wastewater, *Bioresour. Technol.*, 2016, **210**, 123–130.
32 U. R. Lakshmi, V. C. Srivastava, I. D. Mall and D. H. Lataye, Rice husk ash as an effective adsorbent: evaluation of adsorptive characteristics for Indigo Carmine dye, *J. Environ. Manage.*, 2009, **90**, 710–720.
33 E. Gutiérrez-Segura, M. Solache-Rios and A. Colin-Cruz, Sorption of indigo carmine by a Fe-zeolitic tuff and carbonaceous material from pyrolyzed sewage sludge, *J. Hazard. Mater.*, 2009, **170**, 1227–1235.
34 M. Otero, F. Rozada, L. F. Calvo, A. I. Garćıa and A. Morán, Elimination of organic water pollutants using adsorbents obtained from sewage sludge, *Dyes Pigm.*, 2003, **57**, 55–65.
35 M. Dalaran, S. Emik, G. Güçlü, T. B. İyim and S. Özgümüs, Study on a novel polyampholyte nanocomposite superabsorbent hydrogels: synthesis, characterization and investigation of removal of indigo carmine from aqueous solution, *Desalination*, 2011, **279**, 170–182.
36 H. Liu, L. Chen and J. Ding, Adsorption behavior of magnetic amino-functionalized metal–organic framework for cationic and anionic dyes from aqueous solution, *RSC Adv.*, 2016, **6**, 48884–48895.
37 K. Ada, A. Ergene, S. Tan and E. A. Yalc, Adsorption of Remazol Brilliant Blue R using ZnO fine powder: equilibrium, kinetic and thermodynamic modeling studies, *J. Hazard. Mater.*, 2009, **165**, 637–644.
38 S. Lagergren and *Zur theorie der sogenannten., Adsorption geloster stoffe*, Kungliga Svenska Vetenskapsakadem-iens, Handlingar, 1898, vol. 24, pp. 1–39.
39 V. Vimonses, S. M. Lei, B. Jin, C. W. K. Chow and C. Saint, Kinetic study and equilibrium isotherm analysis of Congo Red adsorption by clay materials, *Chem. Eng. J.*, 2009, **148**, 354–364.
40 Y. S. Ho and G. McKay, Pseudo-second order model for sorption processes, *Process Biochem.*, 1999, **34**, 451–465.

